J. Fluid Mech. (1995), *vol.* 299, *pp.* 17–33

Absolute instability of the boundary layer on a rotating disk

By R. J. LINGWOOD

Department of Engineering, University of Cambridge, Trumpington Street, Cambridge CB2 1PZ, UK

(Received 27 July 1994 and in revised form 24 April 1995)

This paper is concerned with the theoretical behaviour of the boundary-layer flow over a disk rotating in otherwise still fluid. The flow is excited impulsively at a certain radius at time $t = 0$. This paper analyses the inviscid stability of the flow and the stability with viscous, Coriolis and streamline curvature effects included. In both cases, within a specific range of the parameter space, it is shown that the flow is *absolutely* unstable, i.e. disturbances grow in time at every fixed point in space. Outside this range, the flow is convectively unstable or stable. The absolute or convective nature of the instabilities is determined by examining the branch-point singularities of the dispersion relation. Absolute instability is found for Reynolds numbers above 510. Experimentally observed values for the onset of transition from laminar to turbulent flow have an average value of 513. It is suggested that absolute instability may cause the onset of transition to turbulent flow. The results from the inviscid analysis show that the absolute instability is not caused by Coriolis effects nor by streamline curvature effects. This indicates that this mechanism may be possible on swept wings, where Coriolis effects are not present but the boundary layers are otherwise similar.

1. Introduction

The present paper analyses the linear stability of the boundary-layer flow over a rotating disk. The boundary layer is similar to that over a swept wing; both boundary layers are three-dimensional with a laminar velocity component that is inflectional. Hence, both flows are susceptible to inviscid *crossflow instability*. The rotating-disk problem has the advantage that there is an exact similarity solution of the Navier–Stokes equations for the base flow, in which the shape of the laminar velocity profiles is independent of the radius. The boundary-layer thickness is also independent of the radius.

It is usual in linear stability analysis to choose either temporal or spatial theories. Temporal theory assumes that the disturbances grow or decay with time from an initial spatial distribution. This implies that the wavenumber is real and that the frequency is complex. Spatial theory, however, assumes that the frequency is real and that the wavenumber is complex. Thus, the disturbances evolve in space from an initial temporal distribution. In order to determine which type of analysis to use, it is necessary to perform a spatio-temporal analysis. This is the approach taken here.

As discussed by Huerre & Monkewitz (1990), the response of the flow to impulsive forcing shows whether it is convectively or absolutely unstable. If the response to the transient disturbance grows with time at a fixed location in space, then the flow is absolutely unstable. Following the work of Briggs (1964) and Bers (1975) in the field of plasma physics, absolute instability can be identified by singularities in the

dispersion relationship that occur when modes associated with waves propagating in opposite directions coalesce. Such points have become known as *pinch-points*. It is known that variation of a parameter, such as the Reynolds number, can cause such points to occur and thus change the behaviour of a flow from a convectively unstable regime to an absolutely unstable regime. Examples of such a change in behaviour are given by Betchov & Criminale (1966) and Koch (1985) for near-wake flows, Brazier-Smith & Scott (1984) for flows over compliant surfaces, Huerre & Monkewitz (1985) for mixing layers with backflow and Niew (1993) for separation bubbles behind backward-facing steps.

It has been suggested (M. Gaster 1992, personal communication) that the rotating-disk boundary layer may also become absolutely unstable. First, the laminar velocity profiles for the rotating-disk boundary layer resolved in directions between the radial and circumferential directions have regions of reverse flow and are similar to those studied by Gaster (1963) and Niew (1993). Reverse mean flow is often thought to be related to absolute instability, since it provides a mechanism for upstream effects. However, as discussed by Huerre & Monkewitz (1990), the wake behind a cylinder that is half immersed in a fluid moving with constant velocity (Triantafyllou & Dimas 1989) has reverse mean flow but is convectively unstable at low Froude numbers. The flow only becomes absolutely unstable in the limit of infinite Froude number. Niew (1993) performed stability calculations on a family of velocity profiles that had varying degrees of reverse flow. He found that the profiles are only absolutely unstable if the region of reverse flow is sufficiently large. Hence, reverse flow is not sufficient for absolute instability but it is present in several absolutely unstable cases.

Secondly, the onset of transition is very repeatable. The visualization experiments performed by Gregory, Stuart & Walker (1955) on the rotating disk showed a region of laminar flow at the centre of the disk followed, at larger radii, by spiral vortices that are stationary with respect to the disk and are caused by roughnesses fixed to the disk. These stationary vortices are now a well-known feature of the flow. At larger radii still, the flow undergoes transition and becomes fully turbulent. Malik, Wilkinson & Orszag (1981) tabulates locations for the onset of transition, as found by various experimentalists, see §5. The values show a scatter of less than 3% around an average Reynolds number of 513, despite various methods of investigation. These results contrast with the onset of transition of the boundary-layer flow on, say, a flat plate, where the onset is sudden but the location is highly dependent on the disturbance environment. This contrast reinforced the idea that a well-defined location of absolute instability of the rotating-disk boundary layer may be triggering the nonlinear behaviour characteristic of the onset of transition. Incidently, there is no reason to associate stationary vortices with absolute instability unless they are growing in time at a fixed point in space.

If there are large roughness elements on the surface of the disk, then the stationary vortices may grow sufficiently to significantly distort the mean velocity profiles, causing secondary instabilities (Kobayashi, Kohama & Takamadate 1980; Kohama 1984, 1987). However, it is assumed in this paper that the wall roughness and the free-stream-turbulence level are both sufficiently small for the transition process to be controlled by the stability of the mean velocity profiles rather than secondary instabilities. Travelling waves (with non-zero frequency) will be considered as well as the usual stationary waves.

The analyses presented in this paper use the parallel-flow approximation (see §§2 and 3) and, therefore, are restricted to the local stability characteristics of the flow. However, as discussed by Huerre & Monkewitz (1990), a region of local absolute

instability may give rise to a self-excited global mode. Generally, it is only the nonlinear results of a global instability that are observable. For example, the limit-cycle oscillations behind a cylinder (the von Kármán vortex street) have been shown to be the result of a global instability (Mathis, Provansal & Boyer 1984). In the case of the rotating-disk boundary layer, it will be shown that the boundary layer becomes locally absolutely unstable above a certain Reynolds number and it is suggested that this results in a global instability and therefore nonlinear behaviour. The close agreement between the onset of absolute instability and the onset of transition observed in experiments (§5) suggests that, in this case, the nonlinearity further destabilizes the boundary layer and promotes transition to turbulence. Experimental results from a study of the behaviour of the rotating-disk boundary layer, which specifically investigates the possibility of an absolute instability and its effects, will be presented at a later date.

In §2 there is a description of the problem and in §3 there is a brief comparison between experimental observations and theoretical results from various analyses. An inviscid linear stability analysis is presented in §4 and in §5 the effects of viscosity, Coriolis and streamline curvature are considered. The conclusions are given in §6.

2. Formulation of the problem

The disk is modelled as an infinite planar disk rotating at a constant angular frequency, Ω^*, about the vertical axis, z^*, which passes through the centre of the disk (asterisks indicate dimensional quantities). The radial and circumferential coordinates are r^* and θ, respectively. The mean flow relative to the disk is given by von Kármán's (1921) exact similarity solution to the Navier–Stokes equations. The dimensionless similarity variables of the solution are defined by

$$U(z) = \frac{U^*}{r^*\Omega^*}, \quad V(z) = \frac{V^*}{r^*\Omega^*}, \quad W(z) = \frac{W^*}{(\nu^*\Omega^*)^{1/2}}, \quad P(z) = \frac{P^*}{\rho^*\nu^*\Omega^*}, \tag{1}$$

where U, V, W are the non-dimensional radial, circumferential and axial base flow velocities, respectively, P is the pressure, ρ^* and ν^* are the density and kinematic viscosity, and $z = z^*/L^*$ is the non-dimensional axial coordinate, where $L^* = (\nu^*/\Omega^*)^{1/2}$ is the non-dimensionalizing lengthscale.

A double-precision fourth-order Runge–Kutta integrator and a Newton–Raphson searching method were used to solve the set of ordinary differential equations (Schlichting 1968) for U, V, W and P. Figure 1(*a*) shows U, V and W plotted against z. The radial velocity profile is inflectional. In directions close to the radial direction the velocity profiles are also inflectional and have regions of reverse flow. The direction is defined in terms of the angle ϵ measured positively from the radial direction in the direction of rotation. The resolved velocity $Q(z)$, where

$$Q(z) = U(z)\cos\epsilon + V(z)\sin\epsilon, \tag{2}$$

is plotted in figure 1(*b*) for $\epsilon = 90°, 45°, 30°, 25°, 20°, 15°, 10°, 5°, 0°$, i.e. ranging from $V(z)$ to $U(z)$ from left to right.

The stability analysis, applied at a radius r_a^*, then involves imposing infinitesimally small disturbances on the mean flow. The local Reynolds number is

$$R = r_a^*\Omega^*L^*/\nu^* = r_a^*/L^* = r_a,$$

and the non-dimensionalizing velocity, pressure and time scales are $r_a^*\Omega^*$, $\rho^* r_a^{*2}\Omega^{*2}$

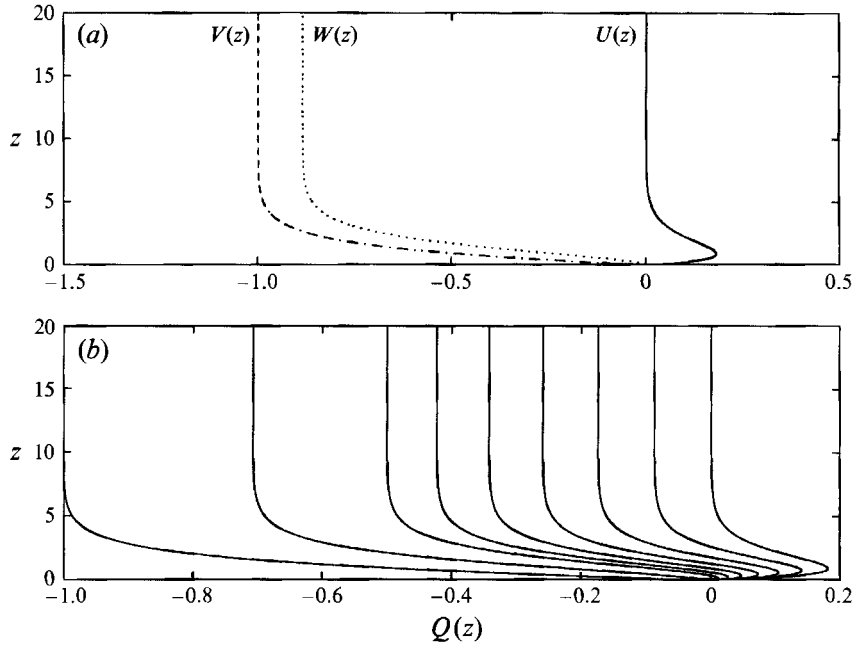

FIGURE 1. Mean velocity profiles: (*a*) $U(z)$, $V(z)$, $W(z)$ plotted against z. $U(z)\to 0$, $V(z)\to -1$ and $W(z)\to -0.8838$. (*b*) $Q(z)$ plotted against z for $\epsilon = 90°, 45°, 30°, 25°, 20°, 15°, 10°, 5°, 0°$, from left to right.

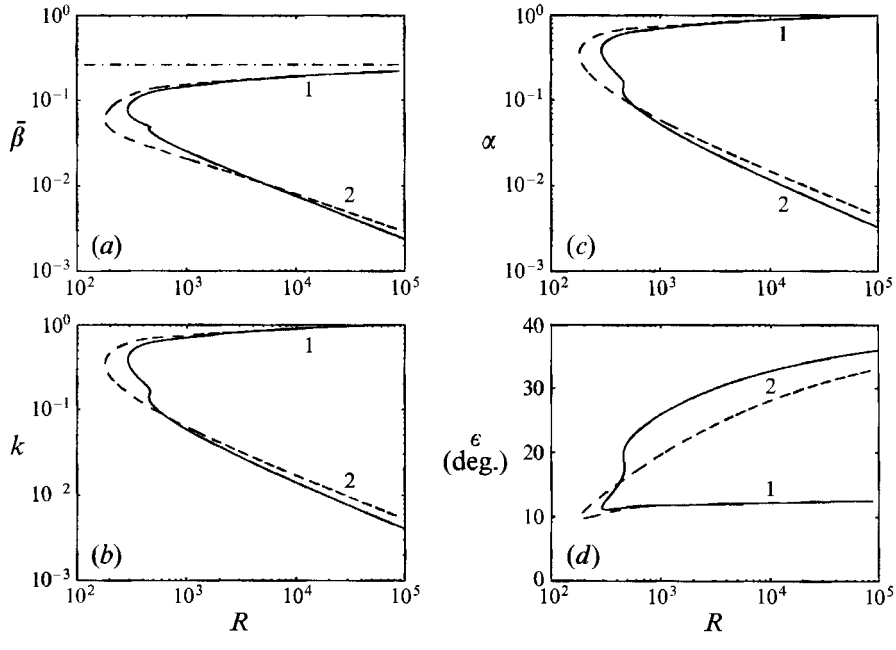

FIGURE 2. Neutral ($\omega_i = 0$, $\alpha_i = 0$) stability diagrams, for stationary modes, calculated from the full sixth-order equations (—) and the fourth-order Orr–Sommerfeld equation (----). The relation $\bar{\beta} = 0.262$ (cf. Gregory *et al.* 1955) (-·-·-) is compared with branch 1. Branches 1 and 2 are marked with their respective numbers.

and $L^*/(\Omega^* r_a^*)$, respectively. The instantaneous non-dimensional velocities and pressure are given by

$$\bar{u}(r,\theta,t,z) = \frac{r}{R}U(z) + u(r,\theta,t,z), \tag{3}$$

$$\bar{v}(r,\theta,t,z) = \frac{r}{R}V(z) + v(r,\theta,t,z), \tag{4}$$

$$\bar{w}(r,\theta,t,z) = \frac{1}{R}W(z) + w(r,\theta,t,z), \tag{5}$$

$$\bar{p}(r,\theta,t,z) = \frac{1}{R^2}P(z) + p(r,\theta,t,z), \tag{6}$$

where u, v, w and p are small perturbation quantities.

The dimensionless Navier–Stokes equations are linearized with respect to the perturbation quantities. In order to make the linearized perturbation equations separable in r, θ and t, it is necessary to ignore variations in the Reynolds number with radius. This involves replacing the variable r, which appears in coefficients of the linearized equations, by R. Despite the fact that the rotating-disk boundary-layer thickness is constant, this sort of approximation is usually called the *parallel-flow* approximation. The terminology comes from analyses of growing boundary layers, such as the Blasius boundary layer, where variations in Reynolds number in the streamwise direction, due to growth of the boundary layer, are often ignored.

Terms $O(R^{-2})$ are neglected and the perturbation quantities are assumed to have normal-mode form

$$\left.\begin{aligned} u &= \hat{u}(z;\alpha,\omega;\beta,R)\,\mathrm{e}^{\mathrm{i}(\alpha r+\beta\theta-\omega t)}, & v &= \hat{v}(z;\alpha,\omega;\beta,R)\,\mathrm{e}^{\mathrm{i}(\alpha r+\beta\theta-\omega t)}, \\ w &= \hat{w}(z;\alpha,\omega;\beta,R)\,\mathrm{e}^{\mathrm{i}(\alpha r+\beta\theta-\omega t)}, & p &= \hat{p}(z;\alpha,\omega;\beta,R)\,\mathrm{e}^{\mathrm{i}(\alpha r+\beta\theta-\omega t)}, \end{aligned}\right\} \tag{7}$$

where $\hat{u}$, $\hat{v}$ and $\hat{w}$ are the spectral representations of the perturbation velocities and $\hat{p}$ is the spectral representation of the perturbation pressure, ω is the frequency of the disturbance in the rotating frame, β is the prescribed integer circumferential wavenumber and α is the radial wavenumber. To distinguish between convectively and absolutely unstable time-asymptotic responses, the initial boundary-value perturbation is provided by an impulsive circumferential line forcing, $\delta(r-r_s)\,\delta(t)\,\mathrm{e}^{\mathrm{i}\beta\theta}$, where $\delta(r-r_s)$ and $\delta(t)$ are the Dirac delta functions at a non-dimensional radius of r_s and at $t=0$, respectively. The response to point forcing can be obtained by summing over all values of β.

The perturbation equations may be written as a set of six first-order ordinary differential equations in the following transformed variables:

$$z_1(z;\alpha,\omega;\beta,R) = (\alpha-\mathrm{i}/R)\,\hat{u} + \bar{\beta}\hat{v}, \tag{8}$$

$$z_2(z;\alpha,\omega;\beta,R) = (\alpha-\mathrm{i}/R)\,\mathrm{D}\hat{u} + \bar{\beta}\mathrm{D}\hat{v}, \tag{9}$$

$$z_3(z;\alpha,\omega;\beta,R) = \hat{w}, \tag{10}$$

$$z_4(z;\alpha,\omega;\beta,R) = \hat{p}, \tag{11}$$

$$z_5(z;\alpha,\omega;\beta,R) = (\alpha-\mathrm{i}/R)\,\hat{v} - \bar{\beta}\hat{u}, \tag{12}$$

$$z_6(z;\alpha,\omega;\beta,R) = (\alpha-\mathrm{i}/R)\,\mathrm{D}\hat{v} - \bar{\beta}\mathrm{D}\hat{u}, \tag{13}$$

where $\bar{\beta} = \beta/R$ and D represents differentiation with respect to z. These equations are

$$Dz_1 = z_2, \tag{14}$$

$$\left[\frac{Dz_2}{R}\right]_v = \frac{1}{R}([\alpha^2+\bar{\beta}^2]_v + iR(\alpha U+\bar{\beta}V-\omega)+U_s)z_1 + \left[\frac{Wz_2}{R}\right]_s + \left(\left(\alpha - \left[\frac{i}{R}\right]_s\right)DU + \bar{\beta}DV\right)z_3 + i\left(\alpha^2+\bar{\beta}^2 - \left[\frac{\alpha i}{R}\right]_s\right)z_4 - \frac{2(l_c+V_s)z_5}{R}, \tag{15}$$

$$Dz_3 = -iz_1, \tag{16}$$

$$Dz_4 = \left[\frac{iWz_1}{R}\right]_s - \left[\frac{iz_2}{R}\right]_v - \frac{1}{R}([\alpha^2+\bar{\beta}^2]_v + iR(\alpha U+\bar{\beta}V-\omega)+DW_s)z_3, \tag{17}$$

$$D_{z_5} = z_6, \tag{18}$$

$$\left[\frac{Dz_6}{R}\right]_v = \frac{2(l_c+V_s)z_1}{R} + \left(\left(\alpha - \left[\frac{i}{R}\right]_s\right)DV - \bar{\beta}DU\right)z_3 + \left[\frac{\bar{\beta}z_4}{R}\right]_s + \frac{1}{R}([\alpha^2+\bar{\beta}^2]_v + iR(\alpha U+\bar{\beta}V-\omega)+U_s)z_5 + \left[\frac{Wz_6}{R}\right]_s, \tag{19}$$

where the subscripts v, c and s indicate which of the $O(R^{-1})$ terms are the viscous, Coriolis and streamline curvature terms, respectively.

If the Coriolis and streamline curvature effects are neglected, the result can be written as the fourth-order Orr–Sommerfeld equation for the rotating disk

$$[i(D^2-\gamma^2)^2 + R(\alpha U+\bar{\beta}V-\omega)(D^2-\gamma^2) - R(\alpha D^2 U+\bar{\beta}D^2 V)]z_3 = 0, \tag{20}$$

where $\gamma^2 = \alpha^2+\bar{\beta}^2$. If all terms of $O(R^{-1})$ are also neglected and viscosity is considered to act only in the establishment of the mean flow, equation (20) reduces to the Rayleigh equation

$$[(\alpha U+\bar{\beta}V-\omega)(D^2-\gamma^2) - (\alpha D^2 U+\bar{\beta}D^2 V)]z_3 = 0. \tag{21}$$

3. Comparison between various analyses and experiment

As stated by Spalart (1990), to apply the parallel-flow approximation over a range of radii implies that the equations are not consistent to $O(R^{-1})$, the same order as the viscous, curvature and Coriolis terms. Therefore, whether using the sixth-order perturbation equations (14)–(19) or the standard Orr–Sommerfeld equation (20), the solutions cannot be justified rigorously at finite Reynolds numbers. However, purely inviscid analyses are rigorous and consistent asymptotic theories can be constructed to account for higher-order terms (Hall 1986; MacKerrell 1987; Bassom & Hall 1990). The following section compares experimental observations with results from inviscid, asymptotic and parallel-flow approximation analyses.

Previous work on the rotation-disk problem has concentrated on the stationary vortex lines, observed in the laminar region prior to transition. There is only a limited number of papers concerning travelling modes (e.g. Bassom & Gajjar 1988; Faller 1991; Bassom & Hall 1991). Therefore, to draw comparisons between various analyses and experimental results, it is necessary to concentrate on studies of the stationary modes in the convectively unstable region.

Figure 2 shows neutral stability curves for stationary modes, i.e. $\alpha_i = \beta_i = \omega_i = 0$ and $\omega_r = 0$ (henceforth, subscripts i and r refer to imaginary and real parts, respectively). The convectively unstable region lies inside the curves. The solid lines were calculated using the viscous sixth-order perturbation equations (14)–(19) and the

broken lines were calculated using the Orr–Sommerfeld equation (20), in which the Coriolis and streamline curvature terms have been neglected. A double-precision fixed-step-size, fourth-order Runge–Kutta integrator was used with Gram–Schmidt orthonormalization and a Newton–Raphson linear search procedure. The wave angle in degrees is given by $\epsilon = \tan^{-1}(\bar{\beta}/\alpha_r)$ and is measured from the outward radial direction in the direction of rotation. The wavenumber resolved in the direction of ϵ is given by $k = (\alpha_r^2 + \bar{\beta}_r^2)^{1/2}$.

Figure 2 shows that the critical Reynolds number for convective instability is significantly lower, about 180, when using the Orr–Sommerfeld equation. This value is consistent with that calculated by Brown (1959) and Cebeci & Stewartson (1980). However, the sixth-order equations give a value of about 290 for the critical Reynolds number, which agrees well with the hot-wire measurements of Malik *et al.* (1981) and Kobayashi *et al.* (1980), who gave values of 294 and 297, respectively. The inclusion of Coriolis and streamline curvature terms has a stabilizing effect and brings the theoretical and experimental results into agreement. As R gets large the upper branch, henceforth known as branch 1, is shown tending towards the asymptotic neutral solution presented by Gregory *et al.* (1955), where $k \approx 1.141$ and $\epsilon \approx 13.3°$. The asymptotic analysis performed by Hall (1986) has shown that the lower branch, henceforth known as branch 2, has a triple-deck structure and is fixed by a balance between viscous and Coriolis forces. Therefore, the lower lobe of the solid curve (branch 2) in figure 2 does not appear when using the Orr–Sommerfeld equation, which neglects the Coriolis terms. In a purely inviscid analysis there is no asymptotic representation of branch 2.

The value of the wave angle calculated in the inviscid limit by Gregory *et al.* (1955) is a fair approximation to the orientation of the stationary vortices observed in experiments. Hall's (1986) asymptotic analysis of branch 1 shows that this close agreement is due to the alternating signs of the higher-order corrections to the inviscid leading-order term. However, the wave angle along branch 2 (figure 2*d*) shows a greater dependence on R and the neglect of Coriolis and streamline curvature effects is significant, especially at low Reynolds numbers.

The inviscid analysis by Gregory *et al.* (1955) showed that the neutral solution for $\omega = 0$ is given by

$$\bar{\beta} = 0.262. \tag{22}$$

This relationship is plotted in figure 2(*a*). At very high Reynolds numbers the agreement with the sixth-order equation results and the Orr–Sommerfeld results is good. It was thought that the value of β for $\omega = 0$ at Reynolds numbers relevant to experiments would be equal to the number of stationary vortices observed in experiments. However, Gregory *et al.* (1955) found that (22) gave about 113 vortices at $R = 430$, and (22) gives about 76 at the critical Reynolds number of about 290, quite different from the 28 to 32 seen in visualization experiments. The reason for this discrepancy is the neglect of viscosity, Coriolis and streamline curvature effects and also that the spiral vortices are not neutral but are growing spatially in the radial direction. Furthermore, the close agreement between the theoretical work by Mack (1985) (based on branch 1 and using a sixth-order viscous analysis with the parallel-flow approximation) and the experimental work by Wilkinson & Malik (1985) has shown that the stationary spiral vortices are the result of the superposition of the complete zero-frequency circumferential wavenumber spectrum and not any single mode. These investigations have shown that randomly distributed roughness elements on the surface of the disk produce individual wave patterns that merge and fill the circumference of the disk, forming the familiar stationary spiral pattern.

Branch 1 stationary vortices are usually observed in experiments. However, Federov *et al.* (1976) observed a mode, using visualization techniques, that had a wave angle of about 20° and gave between 14 and 16 vortices around the disk. These experimental results represent one of very few observations of branch-2 vortices. The nonlinear asymptotic analysis by MacKerrell (1987) suggests that branch-2 vortices are dominant for large-amplitude disturbances but the normally observed branch-1 vortices dominate for small-amplitude disturbances. This suggestion is supported by the theoretical and experimental work of Faller (1991).

To summarize, the linear asymptotic results for branches 1 and 2 agree very well with the results obtained by Malik (1986) above Reynolds numbers of about 10^5 (Hall 1986, figures 2 and 3). Malik (1986) used the parallel-flow approximation and solved the sixth-order perturbation equations. Since the latter approach gives results that agree with the experimental results (e.g. the critical Reynolds number, the wave angle and number of stationary vortices, as discussed above), it seems reasonable to use this approach to study the stability of the flow at Reynolds numbers that are relevant to experiment. Therefore, this is the approach taken in §5 after a consistent inviscid analysis has been presented in §4.

4. Inviscid analysis

Equation (21) is the governing equation for the following inviscid linear stability analysis. The homogeneous boundary conditions to equation (21) are

$$z_3 = 0, \quad z = 0, \qquad z_3 \to 0, \quad z \to \infty. \tag{23}$$

This defines an eigenvalue problem, since (23) can only be satisfied for certain values of α and ω, which give the dispersion relation.

The Rayleigh equation (21) has a singularity at the *critical layer*, where $\alpha U(z_c) + \bar{\beta} V(z_c) - \omega = 0$. The quantity $(\alpha^2 + \bar{\beta}^2)^{1/2}\, \bar{U}(z) = \alpha U(z) + \bar{\beta} V(z)$ is complex when α is complex and ranges from 0 to $-\bar{\beta}$ at $z = 0$ and $z \to \infty$, respectively. The Rayleigh equation (21) has amplified and damped solutions in complex-conjugates pairs. However, physically relevant solutions match onto the solutions of the viscous equations (14)–(19) and (20) for large Reynolds number. Lin (1945*a*, *b*, *c*) showed that to get the appropriate solutions, the path of integration must pass under the singularity if $\mathrm{D}\bar{U}(z_c) > 0$, or over the singularity if $\mathrm{D}\bar{U}(z_c) < 0$. Following a method developed by Healey (1995), this condition was satisfied by calculating $\bar{U}(z)$ and $\mathrm{D}^2\bar{U}(z)$ for complex values of z. The eigenvalues were found using a double-precision fixed-step-size fourth-order Runge–Kutta integrator (using a path of integration that always passed on the correct side of the singularity) and a Newton–Raphson linear search procedure. The solutions at the outer boundary were found analytically from the asymptotic form of (21), assuming that all the perturbations decay exponentially as $z \to \infty$.

The term 'spatial branch' will be used to refer to a locus of solutions of the dispersion relation that lie in the α-plane and are given by a predetermined ω-distribution. These branches are not necessarily purely spatial since ω may be complex. This terminology will be used throughout the paper. Similarly, a branch of the dispersion relation that lies in the ω-plane and is given by a predetermined α-distribution, which may be complex, will be referred to as a 'temporal branch'.

The Briggs (1964) criterion has been applied, with fixed $\bar{\beta}$, to distinguish between convectively and absolutely unstable time-asymptotic responses to the initial boundary-value perturbation, $\delta(\boldsymbol{r} - r_s)\, \delta(t)\, \mathrm{e}^{\mathrm{i}\bar{\beta} r_s \theta}$. The criterion for absolute instability requires a branch-point singularity between two, or more, spatial branches of the dispersion

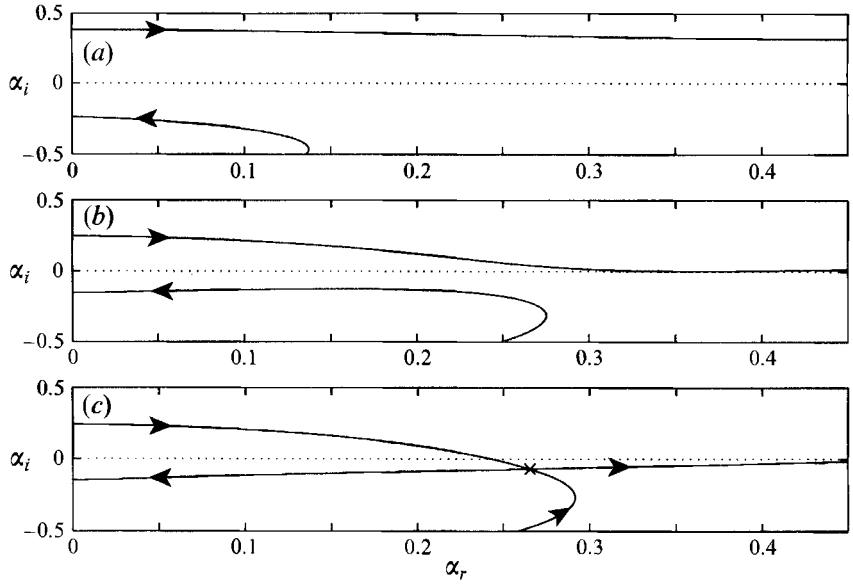

FIGURE 3. The progression of the two spatial branches in the α-plane given by horizontal lines in the ω-plane for $\bar{\beta} = 0.126$: (*a*) $\omega_i = 0.0400$, (*b*) $\omega_i = 0.0150$, (*c*) $\omega_i = \omega_i^o \approx 0.0125$. The pinch-point is marked by a cross ($\times$). The arrows on the spatial branches indicate the direction of increasing ω_r.

relation, of which at least two must lie in distinct half α-planes when ω_i is sufficiently large and positive. Such a singularity has become known as a pinch-point. If $\omega_i > 0$ at the pinch-point the flow is absolutely unstable, otherwise the flow is only convectively unstable or stable. The radial group velocity $\partial\omega/\partial\alpha$ is identically zero at the pinch-point. A branch-point singularity between two spatial branches that lie in the same half α-plane for large positive values of ω_i does not cause absolute instability. Henceforth, the value of ω at a pinch-point will be denoted by ω^o and $\alpha(\omega^o) = \alpha^0$.

These ideas have been applied to different systems and are discussed extensively by Brazier-Smith & Scott (1984), Huerre & Monkewitz (1990) and Chomaz, Huerre & Redekopp (1991), among others.

Discussion and results of the inviscid analysis

Two spatial branches have been found that originate in the distinct half α-planes. It will be shown in § 5 that they match onto two viscous branches at large Reynolds numbers. For $\bar{\beta} = 0.126$, figure 3 shows the two spatial branches, in the α-plane, as ω traces a horizontal line in the ω-plane. Figures 3(*a*), 3(*b*), 3(*c*) show the spatial branches for $\omega_i = 0.0400$, $\omega_i = 0.0150$ and $\omega_i = \omega_i^o \approx 0.0133$, respectively. There is a pinch-point at $\omega = \omega^o \approx -0.0262 + \mathrm{i}0.0133$ and $\alpha = \alpha^o \approx 0.266 - \mathrm{i}0.0670$, as shown in figure 3(*c*), where the flow is absolutely unstable. This discovery and the results from the following viscous analysis, described in § 5, suggest that it may be absolute instability that triggers the onset of transition.

As $\bar{\beta}$ varies, ω^o moves in the complex ω-plane and α^o moves in the complex α-plane; these relationships are shown in figures 4(*a*) and 4(*b*). Figure 4(*c*) shows the variation of the wave angle $\epsilon = \tan^{-1}(\bar{\beta}/\alpha_r^o)$ (in degrees) with $\bar{\beta}$. The ω_i^o-curves of figure 4(*a*) cross the real axis at $\bar{\beta} \approx 0.265$ where $\omega_r^o \approx -0.0698$, $\alpha^o \approx 0.338 - \mathrm{i}0.0582$ and $\epsilon \approx 38.1°$. These points are the upper limits of the region of absolute instability.

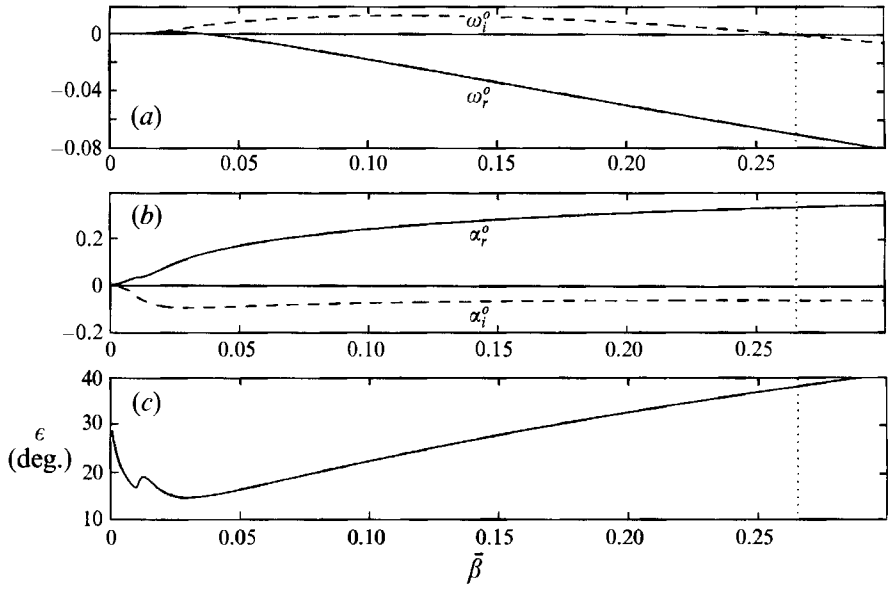

FIGURE 4. (*a*) Locus of the branch-point ω_r^o (—) and ω_i^o (----) as $\bar{\beta}$ varies. (*b*) Locus of the branch-point α_r^o (—) and α_i^o (----) as $\bar{\beta}$ varies. (*c*) Variation in ϵ plotted against $\bar{\beta}$. The dotted line marks the upper limit of the absolutely unstable region.

5. Viscous analysis

In this analysis, equations (14)–(19) are used as the governing perturbation equations. This means that viscous, Coriolis and streamline curvature effects are included. The eigenvalues, α and ω, for fixed R and β were found using a double-precision fixed-step-size fourth-order Runge–Kutta integrator, Gram–Schmidt orthonormalization and a Newton–Raphson linear search procedure. Eigenvalues from the code were compared with those calculated by L. M. Mack (1993, personal communication) and found to agree. The Briggs (1964) criterion, which is summarized in §4, has been applied, with fixed β and R, to distinguish between convectively and absolutely unstable time-asymptotic responses to the initial boundary-value perturbation, $\delta(r-r_s)\,\delta(t)\,e^{i\beta\theta}$.

Discussion and results of the viscous analysis

The branches labelled 1 and 2 on the neutral stability curves in figure 2 and discussed in §3 are the $\omega = 0$ subset of two families of solutions to the dispersion relation. In the following discussion, branches of these two families that relate to travelling waves will also be called branches 1 and 2. Both branches originate in the upper half α-plane when ω_i is large and positive and branch-point singularities have been found between the two. Figure 5 shows branches 1 and 2, in the α-plane, as ω_r traverses a horizontal line in the ω-plane at $R = 515$ and $\beta = 6$, ($\bar{\beta} \approx 0.0117$). Figure 5(*a*), 5(*b*), 5(*c*) show the spatial branches when $\omega_i = 0.01$, 0.004 and 0.0005, respectively. For these particular values of R and β, the branch-point between the two branches happens to occur when $\omega_i \approx 0$, see figure 5(*d*). At the branch-point, where $\omega \approx 0.0243 + i0$ and $\alpha \approx 0.214 - i0.00701$, $\partial\omega/\partial\alpha$ is zero. However, because both branches originate in the upper half α-plane at large positive ω_i, the branch-point does not constitute an absolute instability.

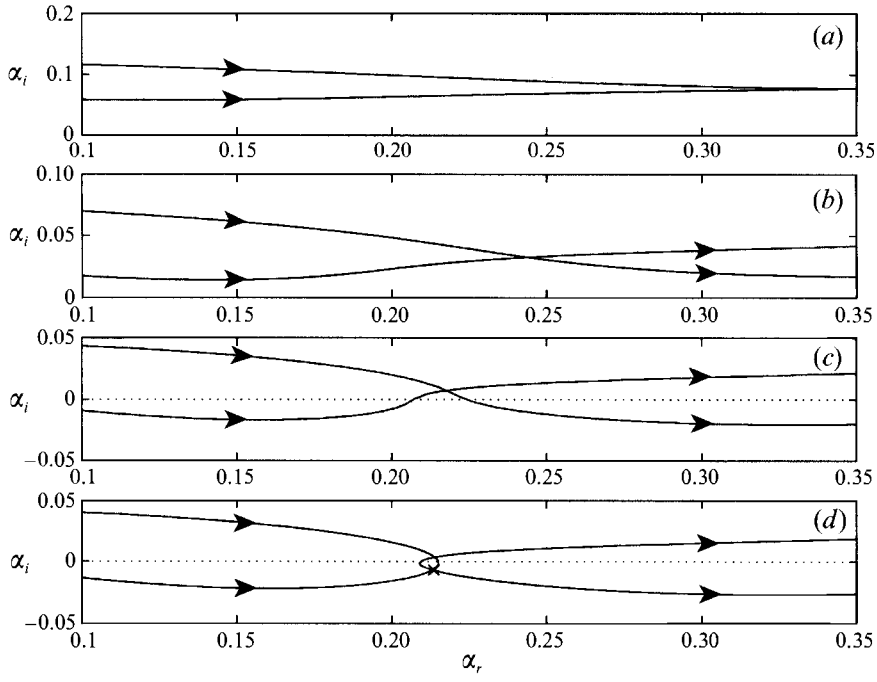

FIGURE 5. The progression of two spatial branches, branches 1 and 2 for $R = 515$ and $\beta = 6$ ($\bar{\beta} \approx 0.0117$), in the α-plane, given by horizontal lines in the ω-plane: (*a*) $\omega_i = 0.01$, (*b*) $\omega_i = 0.004$, (*c*) $\omega_i = 0.0005$, (*d*) $\omega_i = \omega_i^c \approx 0$. The branch-point is marked by a cross (×). The arrows on the spatial branches indicate the direction of increasing ω_r.

Two coalescing spatial branches that originate in the same half α-plane create a second-order pole. For such a case, there is a period of algebraic growth, which may be important if the second-order pole is near neutral, but ultimately the behaviour will be exponential and dictated by the sign of α_i. This case will not be pursued here but has been studied by Koch (1986), Henningson (1991), Henningson, Johansson & Lundbladh (1990) and Henningson, Lundbladh & Johansson (1993).

Neutral stability curves are shown in figure 6 for various real frequencies. Figure 6(*b*) is equivalent to figure 2. The region enclosed by these curves is convectively unstable. The two lobes, observed at positive frequencies, correspond to branches 1 and 2 and the cusps between the two lobes mark the neutral branch-points. As discussed above, these branch-points do not cause absolute instability; however, the curves do show the relative effect of non-zero frequency on the two spatial branches. Positive frequency causes the critical Reynolds number for the onset of convective instability of branch 2 to decrease and that of branch 1 to increase. Negative frequency has the opposite effect: small negative frequencies cause branch 2 to become damped. The sign of the real frequency affects the sign of the phase velocity $[\omega_r/(\alpha_r^2+\bar{\beta}^2)^{1/2}]$, i.e. negative real frequency implies an inward phase velocity. Additionally, the wave angle becomes negative as the frequencies become more positive. The behaviour of branch 2 at increasingly positive frequency shows that branch 2 is the *type-2* instability described by Faller (1991). The type-2 instability, or branch 2, is characterized by a substantially lower critical Reynolds number (Faller 1991 gives a critical value of 69.4 where the wave angle is $-19.0°$), and the radial growth rates are much lower than those of branch 1. Figure 6 in the paper by Faller (1991) shows convective neutral stability

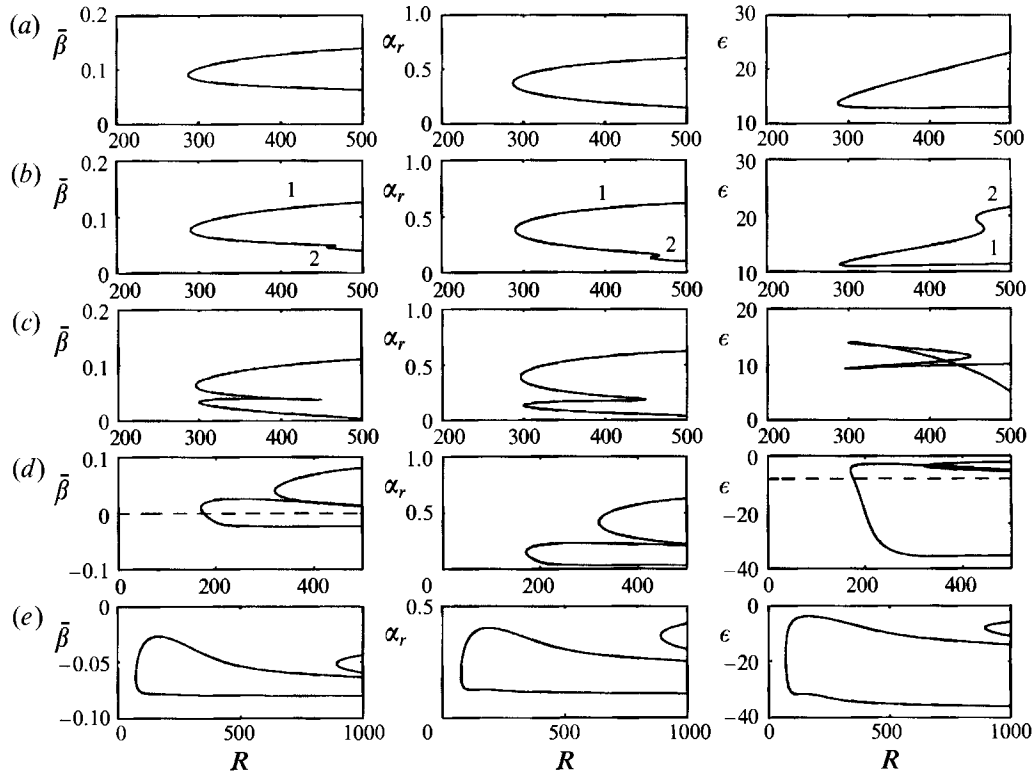

FIGURE 6. Neutral ($\omega_i = 0$, $\alpha_i = 0$) stability diagrams for families 1 and 2: (*a*) $\omega_r = -0.0080$, (*b*) $\omega_r = 0$, (*c*) $\omega_r = 0.0080$, (*d*) $\omega_r = 0.024$, (*e*) $\omega_r = 0.080$. In each case, the neutral curve is shown in the $(\bar{\beta}, R)$-, (α_r, R)- and (ϵ, R)-planes. Branches 1 and 2 are marked with their respective numbers in (*b*), and ϵ is in degrees.

curves non-zero frequency. The figure condenses the information shown here in figure 6, giving one plot in which ω_r varies. It is worth noting that the type-2 instability is analogous to an instability mode found experimentally and theoretically in the Ekman layer, which has been documented by Lilly (1966), Faller & Kaylor (1966) and Tatro & Mollö-Christensen (1967).

The results discussed so far are consistent with the fact that Mack's (1985) calculated wave patterns, based on branch 1, show a convective nature and match the experimentally observed convective region of the flow. It is generally thought that the onset of transition, which is observed experimentally at Reynolds numbers (as tabulated by Malik *et al.* 1981) of about 500 (Kobayashi *et al.* 1980), 505 (Gregory & Walker 1960), 510 (Chin & Litt 1972) and 513–526 (Malik *et al.* 1981), is caused by the radial convective growth of disturbances to amplitudes large enough to cause nonlinearities, perhaps via a secondary instability. A certain amount of variation in the reported transition Reynolds numbers is due to different methods of determination. However, we offer a quite different explanation for transition. Mack (1985) mentions briefly a third spatial branch. Here too, a third branch is found that has the same characteristics as Mack's (1985) branch. It resides in the lower half α-plane for large positive ω_i and therefore corresponds to a response in the region $r < r_s$; it has relatively large negative values of α_i and so is heavily damped. Here, pinch-points between this branch, henceforth called branch 3, and branch 1 have been found. At large positive ω_i these branches lie in the distinct halves of the α-plane and, for certain values of β,

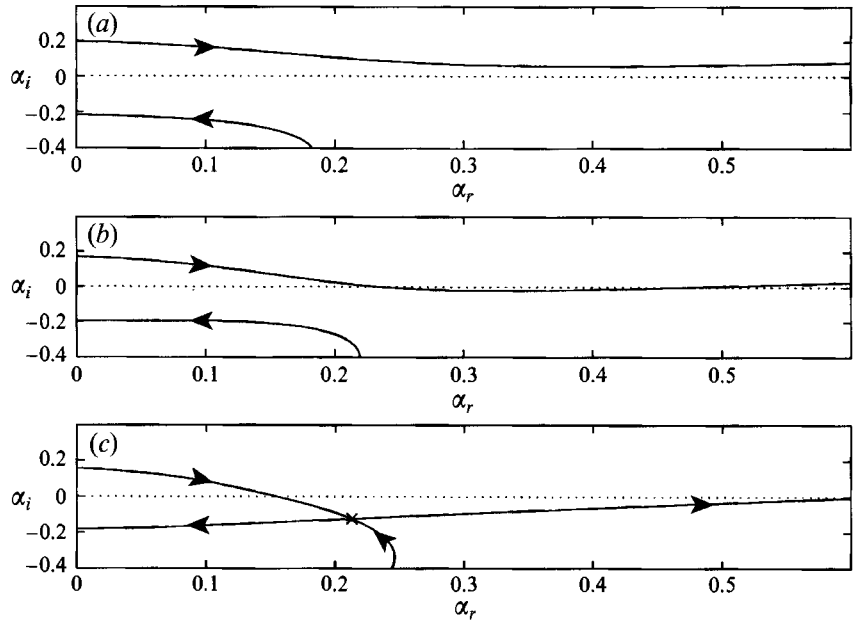

FIGURE 7. The progression of two spatial branches, branches 1 and 3 for $R = 530$ and $\beta = 67$ ($\bar{\beta} \approx 0.126$), in the α-plane given by horizontal lines in the ω-plane: (*a*) $\omega_i = 0.0100$, (*b*) $\omega_i = 0.00400$, (*c*) $\omega_i = \omega_i^o \approx 0.000289$. The pinch-point is marked by a cross (×). The arrows on the spatial branches indicate the direction of increasing ω_r.

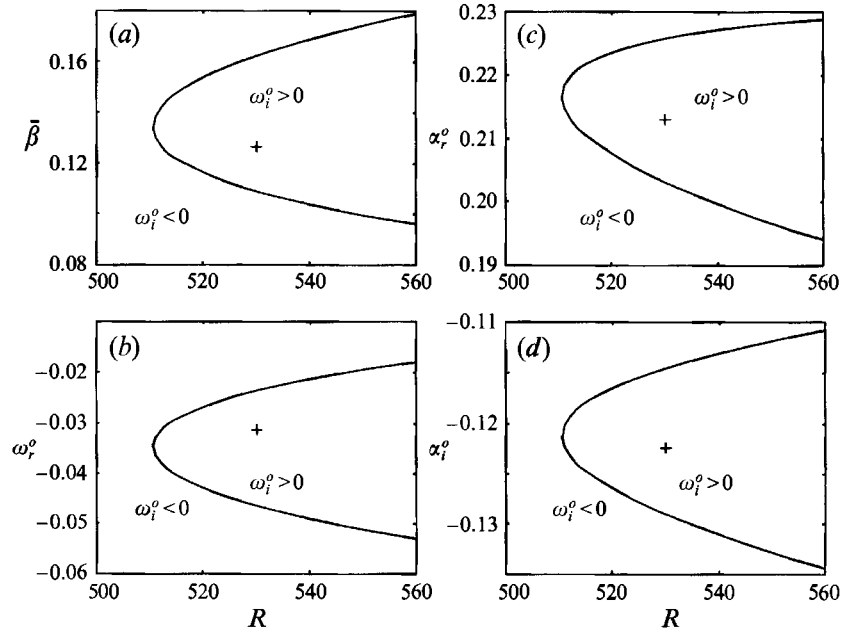

FIGURE 8. Neutral stability curves defining the region of absolute instability. The flow is absolutely unstable within the curves, where $\omega_i^o > 0$. The cross (+) marks the parameters of the particular pinch-point depicted in figure 7.

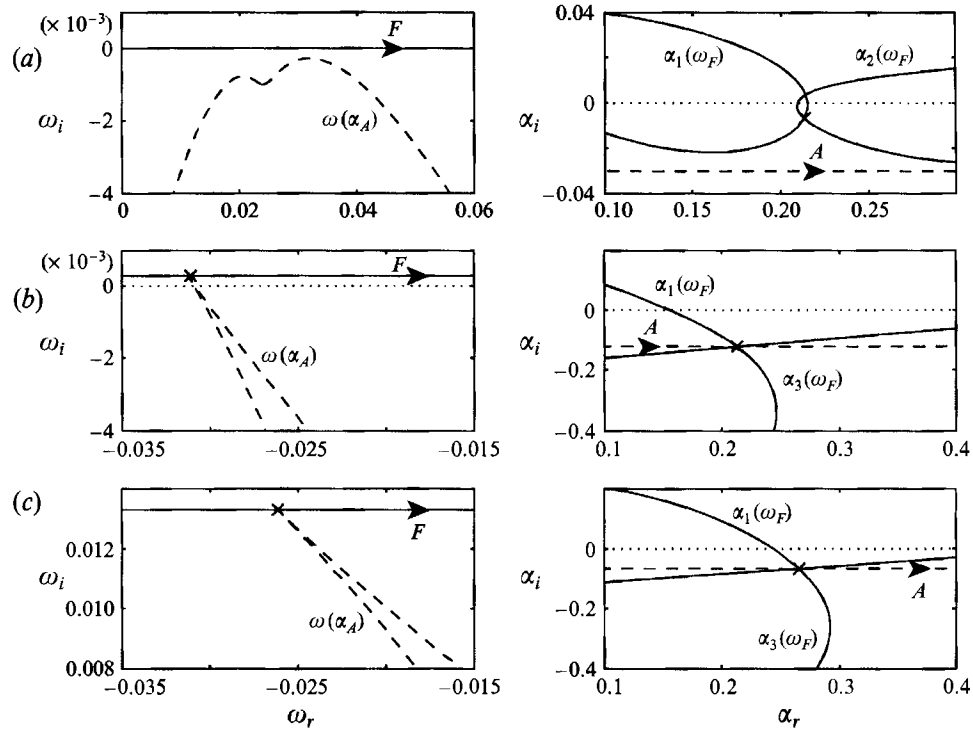

FIGURE 9. (*a*) Viscous temporal branch in the ω-plane (given by the A-line) and viscous spatial branches 1 and 2 in the α-plane (given by the F-line), for $R = 515$ and $\beta = 6$ ($\bar{\beta} \approx 0.0117$), showing the branch-point. (*b*) Viscous temporal branch in the ω-plane and viscous spatial branches 1 and 3 in the α-plane, for $R = 530$ and $\beta = 67$ ($\bar{\beta} \approx 0.126$), showing the pinch-point. (*c*) Inviscid temporal branch in the ω-plane and inviscid spatial branches 1 and 3 in the α-plane, for $\bar{\beta} = 0.126$, showing the pinch-point.

above a critical Reynolds number of 510.625, ω_i^o at the pinch-point is positive. These points correspond to absolute instabilities. Such an example is shown in figure 7, in which branches 1 and 3 are shown in the α-plane, at $R = 530$ and $\beta = 67$ ($\bar{\beta} \approx 0.126$). Figures 7(*a*) and 7(*b*) show the branches when $\omega_i = 0.0100$ and 0.00400, respectively. Figure 7(*c*) shows the pinch-point at $\omega^o \approx -0.0311 + \mathrm{i}0.000289$ and $\alpha^o \approx 0.213 - \mathrm{i}0.123$, where the wave angle $\epsilon \approx 30.7°$. Below $R = 510.625$, ω_i can be reduced to zero before pinching occurs and the flow is then only convectively unstable. Note the similarity between the viscous results in figure 7 and the inviscid results in figure 3.

Figure 8 shows the neutral stability curves for absolute instability in the $(R, \bar{\beta})$-, (R, ω_r^o)-, (R, α_r^o)- and (R, α_i^o)-planes. Inside the stability curves ω_i^o is positive and outside it is negative. The absolutely unstable region lies within the curves and the parameter region over which the flow is absolutely unstable is shown to expand at Reynolds numbers above the critical value. The maximum magnitude of ω_i^o also increases with increasing R. Since branch 1 moves into the lower half α-plane to meet branch 3 at the pinch-points, the region of absolute instability must lie within the region of convective instability for branch 1.

The structure of a normal branch-point compared with a pinch-point is shown graphically in figures 9(*a*) and 9(*b*). Figure 9 also shows a comparison between an absolutely unstable pinch-point ($\omega_i^o > 0$) from the viscous analysis (figure 9*b*) and from the inviscid analysis (figure 9*c*); the value of $\bar{\beta}$ is 0.126 in both cases. Figure 9(*a*) shows

the same case as figure 5(*d*), figure 9(*b*) is the same case as figure 7(*c*) and figure 9(*c*) is the same case as figure 3(*c*). The temporal branch given by the values of α along the line marked A in figure 9 is denoted by $\omega(\alpha_A)$. Similarly, the spatial branches given by the values of ω along the line marked F are denoted by $\alpha(\omega_F)$. When $\omega(\alpha_A)$ is plotted in the complex ω-plane, both the viscous and the inviscid pinch-points show a characteristic cusp at ω_i^o (figure 9*b*, *c*). This characteristic has been used by Kupfer, Bers & Ram (1987) to locate points of absolute instability. Apart from the magnitude of ω_i^o, the parameter values at the inviscid and viscous pinch-points are very similar. Indeed, since ω_i^o increases with increasing Reynolds number, the viscous results will approach the inviscid results at large Reynolds number. This agreement between figure 9(*b*) and 9(*c*) confirms that the two inviscid spatial branches are the asymptotic limits of branches 1 and 3 at infinite Reynolds number. Since branch 2 does not appear in inviscid analyses (see §3), there are no inviscid branch-points of the type shown in figure 5(*d*) and 9(*a*), where the two spatial branches originate in the same half-plane at large ω_i.

6. Conclusions

The disturbances on a rotating disk have been investigated using linear stability theory. The general convective nature of much of the flow is already known, but this investigation has focused on the possibility of an absolute instability occurring in some parameter range. Given sufficient time, even a weakly absolutely unstable flow will cause a disturbance at a fixed point in space to grow to amplitudes large enough to make the use of linear theory invalid. In contrast, a disturbance in a convectively unstable flow is swept away as it grows, and the source area is ultimately left undisturbed, and so the boundary layer remains basically laminar until the instability wave has travelled far enough away to have grown to amplitudes sufficient to cause nonlinearities. Hence, absolute instability is quite distinct from spatial instability and is far more dangerous. Furthermore, the presence of an absolute instability would imply that any asymptotic stability analysis should be temporal as well as spatial.

Firstly, all terms of $O(R^{-1})$ were neglected, giving a consistent set of linearized perturbation equations, i.e. the three-dimensional Rayleigh equation. The boundary layer was found to be radially absolutely unstable over a range of $\bar{\beta}$. Secondly, a linear stability analysis has been performed on the sixth-order perturbation equations that include viscous, Coriolis and streamline curvature effects. A third damped branch of the dispersion relation has been shown to meet branch 1 at pinch-points with positive ω_i. These points indicate radial absolute instability for $R > 510.625$ and suitable β. Below the critical Reynolds number, the flow is convectively unstable or stable depending on the parameter values. Neutral stability curves are presented that show the absolutely unstable, convectively unstable and stable regions.

It is known that inviscid crossflow instability destabilizes boundary layers. Hence, the transition mechanism for the rotating-disk boundary layer could be expected to be inviscid. Therefore, it is encouraging that the results presented in §4 show that the absolute instability is an inviscid mechanism. Furthermore, the onset of absolute instability is consistent with experimental observations of the critical Reynolds number for the onset of transition ($513 \pm 3\%$, cf. §5). Although the parallel-flow approximation in the viscous analysis will have some small numerical effect on the stability calculations, the general absolute instability characteristics discussed in this paper are still relevant to the physical behaviour of the flow. Therefore, absolute instability may be a better explanation for transition than the convective radial growth of disturbances,

leading to nonlinearity. Moreover, this mechanism may be relevant to transition on highly swept wings.

This work has benefited from discussions with Professor M. Gaster, Professor D. G. Crighton and Dr J. J. Healey. I am grateful to Dr L. M. Mack for advice on the Gram–Schmidt orthonormalization technique. This work was supported by the Engineering and Physical Sciences Research Council and the Boeing Commercial Airplane Group.

REFERENCES

BASSOM, A. P. & GAJJAR, J. S. B. 1988 Non-stationary cross-flow vortices in three-dimensional boundary-layer flows. *Proc. R. Soc. Lond.* A **417**, 179–212.

BASSOM, A. P. & HALL, P. 1990 On the interaction of stationary crossflow vortices and Tollmien–Schlichting waves in the boundary layer on a rotating disc. *Proc. R. Soc. Lond.* A **25**, 25–55.

BASSOM, A. P. & HALL, P. 1991 Concerning the interaction of non-stationary crossflow vortices in a three-dimensional boundary layer. *Q. J. Mech. Appl. Maths* **44**, 147–172.

BERS, A. 1975 Linear waves and instabilities. In *Physique des Plasmas* (ed. C. DeWitt & J. Peyraud), pp. 117–215. Gordon & Breach.

BETCHOV, R. & CRIMINALE, W. O. 1966 Spatial instability of the inviscid jet and wake. *Phys. Fluids* **9**, 359–362.

BRAZIER-SMITH, P. R. & SCOTT, J. F. 1984 Stability of fluid flow in the presence of a compliant surface. *Wave Motion* **6**, 547–560.

BRIGGS, R. J. 1964 *Electron-Stream Interaction with Plasmas*. MIT Press.

BROWN, W. B. 1959 Numerical calculation of the stability of cross flow profiles in laminar boundary layers on the rotating disc and on a swept wing and an exact calculation of the stability of the Blasius velocity profile. *Rep.* Northrop Aircraft Inc., Hawthorne, CA.

CEBECI, T. & STEWARTSON, K. 1980 Stability and transition in three-dimensional flows. *AIAA J.* **18**, 398–405.

CHIN, D. & LITT, M. 1972 An electrochemical study of flow instability on a rotating disk. *J. Fluid Mech.* **54**, 613–625.

CHOMAZ, J. M., HUERRE, P. & REDEKOPP, L. G. 1991 A frequency selection criterion in spatially developing flows. *Stud. Appl. Maths* **84**, 119–144.

FALLER, A. J. 1991 Instability and transition of the disturbed flow over a rotating disk. *J. Fluid Mech.* **230**, 245–269.

FALLER, A. J. & KAYLOR, R. E. 1966 A numerical study of the instability of the laminar Ekman boundary layer. *J. Atmos. Sci.* **23**, 466–480.

FEDOROV, B. I., PLAVNIK, G. Z., PROKHOROV, I. V. & ZHUKHOVITSKII, L. G. 1976 Transitional flow conditions on a rotating disk. *J. Engng Phys.* **31**, 1448–1453.

GASTER, M. 1963 On stability of parallel flows and the behaviour of separation bubbles. PhD thesis, Queen Mary College, London.

GREGORY, N., STUART, J. T. & WALKER, W. S. 1955 On the stability of three-dimensional boundary layers with application to the flow due to a rotating disk. *Phil. Trans. R. Soc. Lond.* A **248**, 155–199.

GREGORY, N. & WALKER, W. S. 1960 Experiments on the effect of suction on the flow due to a rotating disk. *J. Fluid Mech.* **9**, 225–234.

HALL, P. 1986 An asymptotic investigation of the stationary modes of the instability of the boundary layer on a rotating disc. *Proc. R. Soc. Lond.* A **406**, 93–106.

HEALEY, J. J. 1995 A comparison between Orr–Sommerfeld theory and asymptotic theories for damped and growing boundary layer modes. *J. Fluid Mech.* (submitted).

HENNINGSON, D. S. 1991 An eigenfunction expansion of localized disturbances. *Advances in Turbulence 3* (ed. A. V. Johansson & P. H. Alfredsson), pp. 162–169. Springer.

HENNINGSON, D. S., JOHANSSON, A. V. & LUNDBLADH, A. 1990 On the evolution of localized disturbances in laminar shear flows. In *Laminar-Turbulent Transition* (ed. D. Arnal & R. Michel), pp. 279–284. Springer.

HENNINGSON, D. S., LUNDBLADH, A. & JOHANSSON, A. V. 1993 A mechanism for bypass transition from localized disturbances in wall-bounded shear flows. *J. Fluid Mech.* **250**, 169–207.

HUERRE, P. & MONKEWITZ, P. A. 1985 Absolute and convective instabilities in free shear layers. *J. Fluid Mech.* **159**, 151–168.

HUERRE, P. & MONKEWITZ, P. A. 1990 Local and global instabilities in spatially developing flows. *Ann. Rev. Fluid Mech.* **22**, 473–537.

KÁRMÁN, TH. VON 1921 Über laminare und turbulente Reibung. *Z. Angew. Math. Mech.* **1**, 233–252.

KOBAYASHI, R., KOHAMA, Y. & TAKAMADATE, CH. 1980 Spiral vortices in boundary layer transition regime on a rotating disk. *Acta Mech.* **35**, 71–82.

KOCH, W. 1985 Local instability characteristics and frequency determination of self excited wake flows. *J. Sound Vib.* **99**, 53–83.

KOCH, W. 1986 Direct resonance in Orr–Sommerfeld problems. *Acta Mech.* **58**, 11–29.

KOHAMA, Y. 1984 Study on boundary layer transition of a rotating disk. *Acta Mech.* **50**, 193–199.

KOHAMA, Y. 1987 Crossflow instability in rotating disk boundary layer. *AIAA Paper* 87-1340.

KUPFER, K., BERS, A. & RAM, A. K. 1987 The cusp map in the complex-frequency plane for absolute instabilities. *Phys. Fluids* **30**, 3075–3082.

LILLY, D. K. 1966 On the instability of Ekman boundary flow. *J. Atmos. Sci.* **23**, 481–494.

LIN, C. C. 1945*a* On stability of two-dimensional parallel flows, Part I. *Q. appl. Math.* **3**, 117–142.

LIN, C. C. 1945*b* On stability of two-dimensional parallel flows, Part II. *Q. appl. Math* **3**, 218–234.

LIN, C. C. 1945*c* On stability of two-dimensional parallel flows, Part III. *Q. appl. Math* **3**, 277–301.

MACK, L. M. 1985 The wave pattern produced by point source on a rotating disk. *AIAA Paper* 85-0490.

MACKERRELL, S. 1987 A nonlinear, asymptotic investigation of the stationary modes of instability of the three-dimensional boundary layer on a rotating disc. *Proc. R. Soc. Lond.* A **413**, 497–513.

MALIK, M. R. 1986 The neutral curve for stationary disturbances in rotating-disk flow. *J. Fluid Mech.* **164**, 275–287.

MALIK, M. R., WILKINSON, S. P. & ORSZAG, S. A. 1981 Instability and transition in rotating disk flow. *AIAA J.* **19**, 1131–1138.

MATHIS, C., PROVANSAL, M. & BOYER, L. 1984 The Bénard–von Kármán instability: an experimental study near the threshold. *J. Phys. (Paris) Lett.* **45**, 483–491.

NIEW, T. R. 1993 The stability of the flow in a laminar separation bubble. PhD thesis, Cambridge University.

SCHLICHTING, H. 1968 *Boundary-Layer Theory*, Sixth edn., pp. 93–96. McGraw-Hill.

SPALART, P. R. 1990 Direct numerical study of crossflow instability. In *Laminar-Turbulent Transition* (ed. D. Arnal & R. Michel), pp. 621–630. Springer.

TATRO, P. R. & MOLLÖ-CHRISTENSEN, E. L. 1967 Experiments on Ekman layer instability. *J. Fluid Mech.* **28**, 531–543.

TRIANTAFYLLOU, G. S. & DIMAS, A. 1989 The low Froude number wake of floating bluff objects. *Intern. Rep.* MITSG 89-5, MIT, Cambridge.

WILKINSON, S. P. & MALIK, M. R. 1985 Stability experiments in the flow over a rotating disk. *AIAA J.* **21**, 588–595.